

Supplement

Marine Remaud

Correspondence: marine.remaud@lsce.ipsl.fr

A GPP estimates

GPP Estimate (PgC/yr) +/- SD	Method	Duration (Years)	Citation
110 +/- 11	MODIS	1982-2012	Zhao et al.
128 +/- 4	Neural Network	1998-2005	Beer et al.
124 +/- 7	Water Use Efficiency	1998-2005	Beer et al.
106 +/- 6	Light Use Efficiency	1998-2005	Beer et al.
119 +/- 6	Upscaled Flux Tower	1982-2008	Jung et al.
129 +/- 16	Oxygen isotopes in H ₂ O	1968-2013	Jaschko et al.
162.5 +/- 6	Oxygen isotopes in CO ₂	1990-2010	Welp et al.
122 +/- 2.4	Solar Induced Fluorescence (WE CAN)	2010-2015	Alemohammad
125 +/- 12	Process BESS Model	1982-2015	Ryu et al.
147 +/- 8	Near Infrared (NIR)		Badgley et al.
125 +/- 5.2	<i>MODIS</i> soil moisture constrained	1982-2016	Stocker et al.
130 +/- 17	<i>Inverse Variance Weighted Estimate</i>		

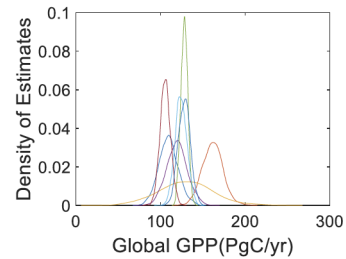


Figure S1. Left: compilation of GGP estimates from recent litterature. Right: Distribution of these GPP estimates, assuming they are gaussian with a standard deviation equal to the uncertainties on the tabular. From Ashley Ballentyne personnal presentation

B Evaluation of the reconstructed adjoint transport

We check here that the reconstructed transport using the adjoint transport is consistent with the full LMDz transport. Figure S2 shows a comparison of the CO₂ concentrations given by the adjoint of LMDz against concentrations simulated by the forward 5 LMDz ATM at surface. The adjoint transport and the forward model are in almost total agreement at all stations.

CO₂

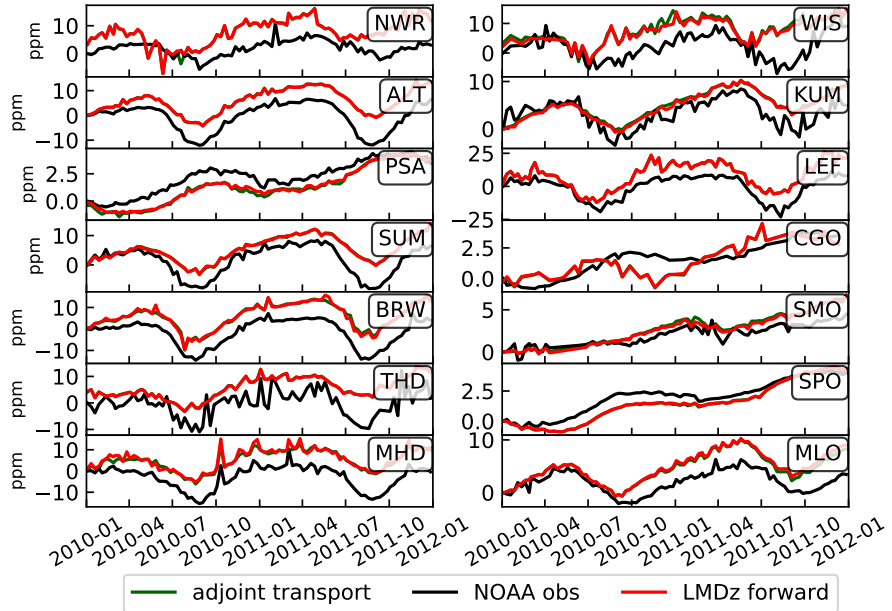


Figure S2. Temporal series of observed (black) and simulated CO_2 (green and red) concentrations at surface sites from the NOAA network. The red curve corresponds to the concentrations simulated by the full atmospheric transport. The green curve corresponds to the concentrations given by backward integration of the adjoint transport combined to the prior fluxes (reconstructed transport).

C Prior and posterior CO₂ and COS budgets

CO ₂ GPP [GtC/y]			CO ₂ Respiration [GtC/y]		
PFT	Prior	Post	PFT	Prior	Post
10 TeC3g	-4.9	-3.7	1 BaSoil	0.2	0.2
11 C4g	-19.0	-19.0	10 TeC3g	5.4	4.6
12 C3Ag	-15.3	-15.3	11 C4g	19.6	17.0
13 C4Ag	-7.1	-7.0	12 C3Ag	13.4	9.8
14 TrC3g	-1.7	-1.6	13 C4Ag	5.8	5.3
15 BoC3g	-4.5	-4.3	14 TrC3g	2.1	2.0
2 TrBrE	-35.7	-33.3	15 BoC3g	4.7	5.3
3 TrBrR	-10.4	-9.2	2 TrBrE	35.8	35.1
4 TeNeE	-4.0	-3.0	3 TrBrR	10.4	9.9
5 TeBrE	-6.1	-4.8	4 TeNeE	4.0	4.1
6 TeBrS	-5.5	-4.9	5 TeBrE	6.1	5.4
7 BoNeE	-5.8	-7.2	6 TeBrS	5.4	4.7
8 BoBrS	-3.8	-4.3	7 BoNeE	5.5	5.3
9 BoNeS	-1.3	-1.5	8 BoBrS	3.6	3.7
			9 BoNeS	1.2	1.1

Vegetation sink [GgS/y]			COS Soil fluxes [GgS/y]		
PFT	Prior	Post	PFT	Prior	Post
10 TeC3g	-27.4	-20.6	10 TeC3g	-21.0	-15.1
11 C4g	-77.3	-77.1	11 C4g	-25.9	-24.6
12 C3Ag	-85.6	-84.8	12 C3Ag	-11.3	-11.0
13 C4Ag	-28.4	-27.9	13 C4Ag	-1.5	-1.5
14 TrC3g	-9.7	-8.7	14 TrC3g	-17.7	-15.7
15 BoC3g	-24.9	-23.8	15 BoC3g	-33.3	-31.2
2 TrBrE	-201.6	-187.9	2 TrBrE	-24.0	-21.3
3 TrBrR	-59.1	-51.8	3 TrBrR	-21.3	-18.9
4 TeNeE	-22.0	-16.6	4 TeNeE	-12.3	-9.7
5 TeBrE	-34.2	-26.8	5 TeBrE	-12.0	-9.1
6 TeBrS	-30.7	-27.3	6 TeBrS	-14.6	-11.7
7 BoNeE	-32.3	-39.9	7 BoNeE	-18.0	-17.1
8 BoBrS	-21.1	-23.7	8 BoBrS	-14.4	-14.0
9 BoNeS	-7.1	-8.4	9 BoNeS	-9.7	-9.5

Figure S3. Top: Distribution of the average total yearly GPP and respiration per PFT in GtC Bottom: Distribution of the average total yearly vegetation and soil COS fluxes per PFT in GgS

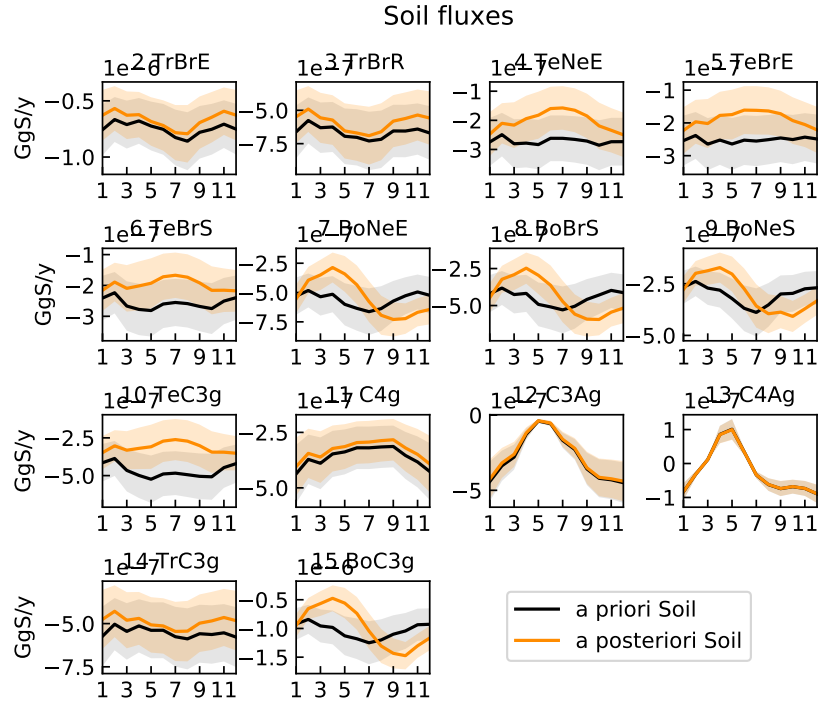


Figure S4. Mean seasonal cycle of the total prior (black) and posterior (orange) soil fluxes and their uncertainties within each of the 15 PFTs. The fluxes have been averaged between 2009-2011. Only the values integrated over the Northern Hemisphere are shown for the PFTs 4, 5, 6, 10, 11, 12, 13.

D Supplementary figures of the section 3.3.2 : Evaluation of the simulated vertical profiles against NOAA/ESRL airborne measurements

The used observation programme here is the NOAA Earth System Research Laboratory (ESRL) Global Greenhouse Gas Reference Network Aircraft Program. It provides information about the vertical profiles of CO_2 and COS (Montzka et al., 5 2007; Campbell et al., 2008; Ma et al., 2020). It consists here of measurements of air samples collected by flasks every few days or months at 16 aircraft profiling sites over continental and coastal North America between 2008 and 2011 between altitudes of 300 and 8000 m above sea level.

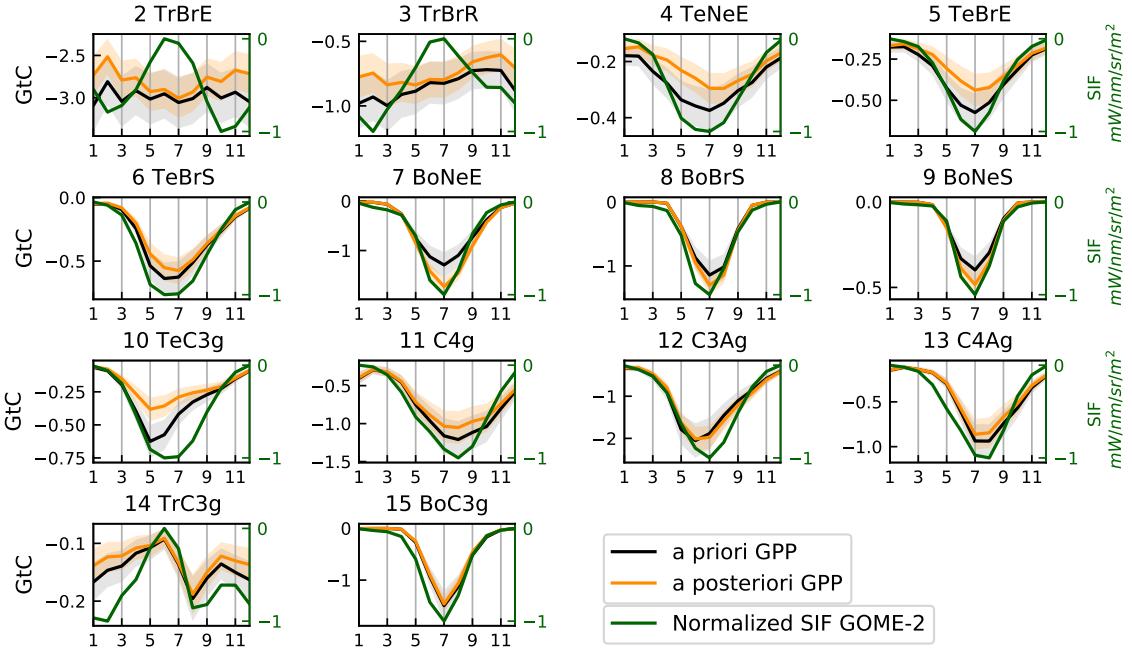


Figure S5. Mean seasonal cycle of the total prior (black) and posterior (orange) GPP fluxes and their uncertainties within each of the 15 PFTs during the period 2009–2018. The mean seasonal cycle of the SIF from GOME-2 has been superimposed on the GPP seasonal cycle in green. The fluxes have been averaged between 2009–2018. PFT 1, the bare soil, is not shown as respiration and GPP are null. Only the values integrated over the Northern Hemisphere are shown for PFTs 4, 5, 6, 10, 11, 12 and 13. The acronyms Tr, Bo and Te mean Tropical, Boreal and Temperate, respectively.

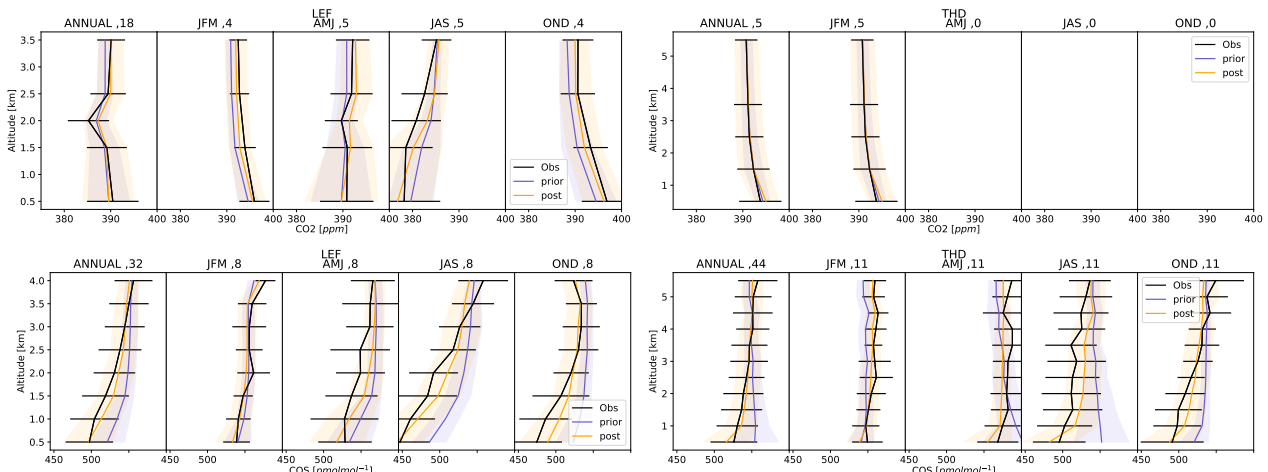


Figure S6. Mean (thick lines) and associated standard deviation (shaded areas) for the monthly CO₂ (top) and COS (Bottom) vertical profile at site LEF (left) and THD (right) during the period 2008–2011. The data have first been averaged in 0.5 km altitude bins per hour and per site. The statistics are drawn from that ensemble of monthly averaged values. They are shown for each season (January–March, JFM; April–June, AMJ; July–September, JAS; October–December, OND) and for the whole year. In order to highlight the differences in profile shape, the annual mean of the bias at 3.5 km has been removed for the prior vertical profile.

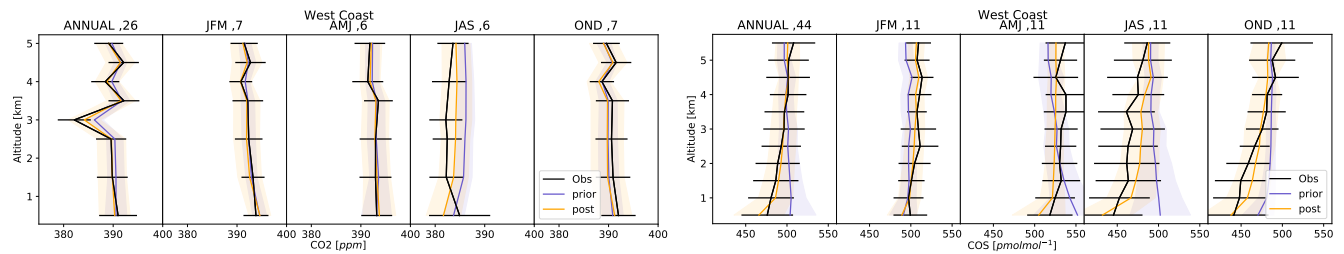


Figure S7. Same Figure as S6 but for the West Coast domain. The West Coast domain is associated with the ESP site.

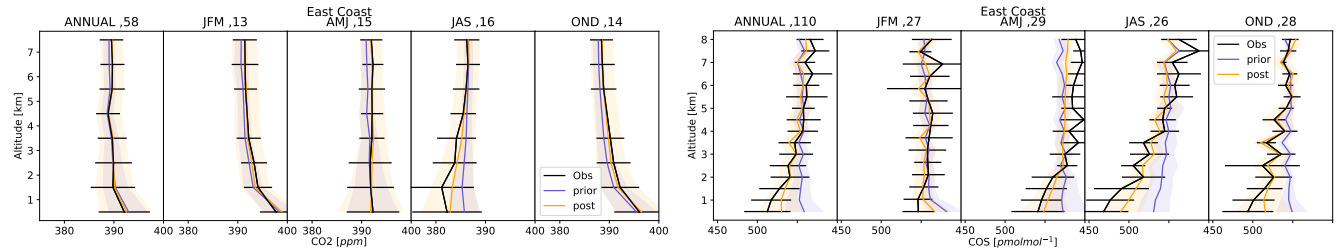


Figure S8. Same Figure as S6 but for the East Coast domain. The East Coast domain encompasses the NHA and CMA.

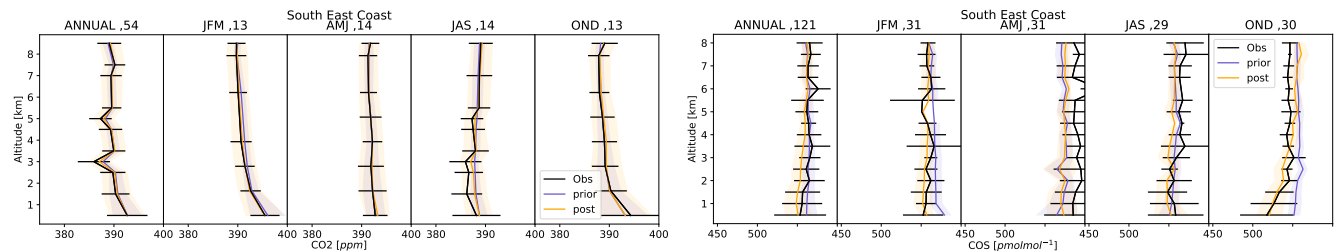


Figure S9. Same Figure as S6 but for the South East Coast domain. The South East Coast domain encompasses the sites SCA and TGC.

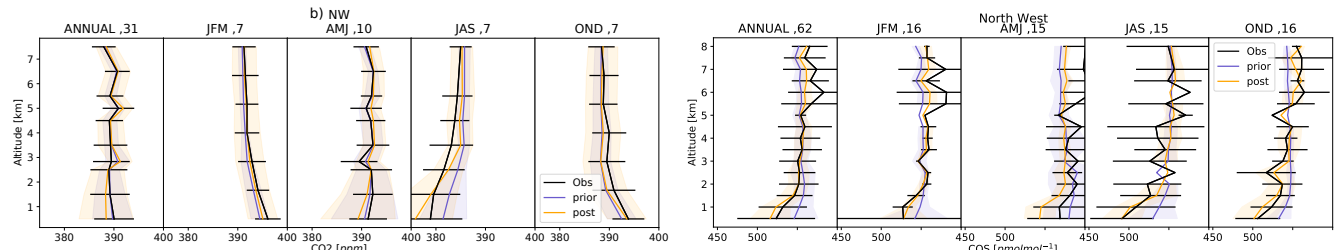


Figure S10. Same Figure as S6 but for the North West domain. The North West domain is associated with the site ETL.

E Supplementary figures of the section 3.3.2 : Evaluation of the simulated concentrations against surface measurements at three Japanese sites.

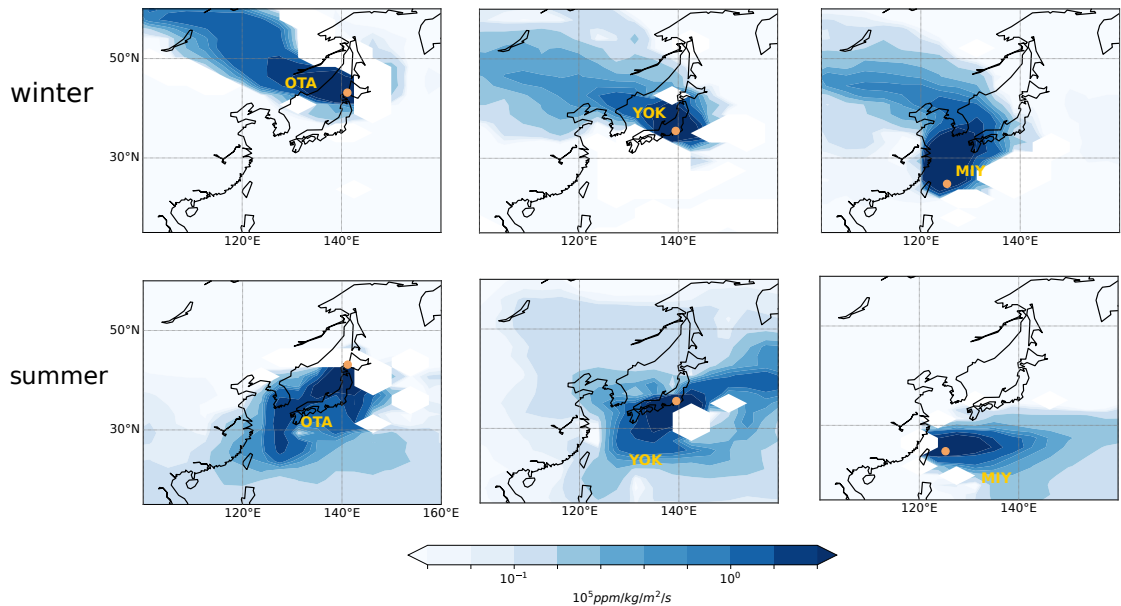


Figure S11. Seasonal climatology (Winter: top and Summer: bottom) of the Jacobians computed by the adjoint of the LMDz model: map of the partial derivatives, in $\text{ppm}/(\text{kg}/\text{m}^2/\text{h})$, of a weekly mean concentration for the station OTA (left), YOK (middle), MIY (right) with respect to CO₂ surface fluxes in the previous month. The yellow dots denote the location of the surface sites. The white areas corresponds to negative sensitivities resulting from the slope limiters introduced in the Van Leer (1977) advection scheme (see Hourdin et al. (2006) for more explanations.)

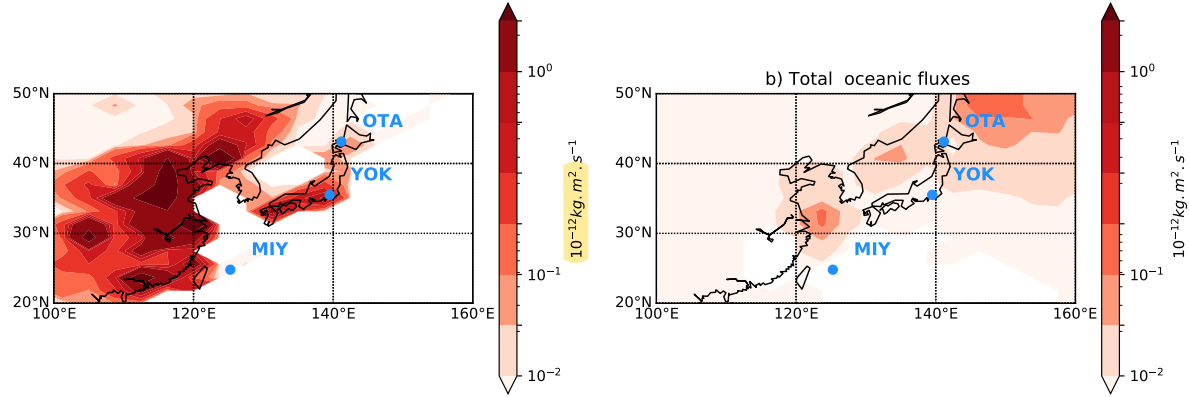


Figure S12. a) Anthropogenic emission map and b) Prior oceanic emission map for summer 2019 (July-August). The blue dots denote the location of the surface sites. The anthropogenic fluxes have been interpolated on the coarser LMDz grid while ensuring mass conservation and therefore don't follow exactly to the `python` coastlines. The fluxes are the reference fluxes described in section 2.

F Supplementary figures of the section 3.3.2 : Evaluation of the simulated concentrations against surface measurements at GIF

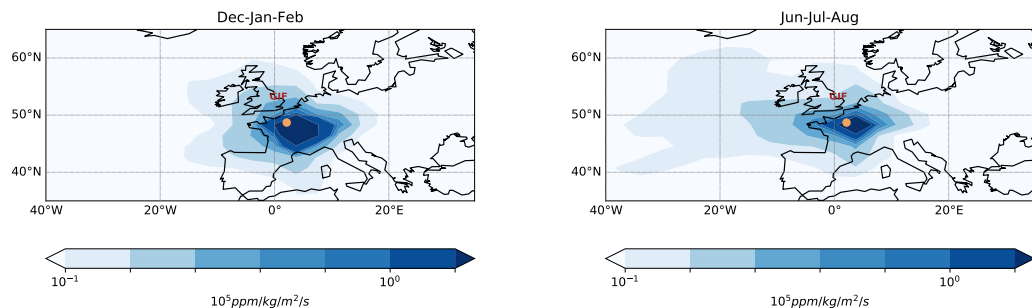


Figure S13. Seasonal climatology (Winter: left and Summer: right) of the Jacobians computed by the adjoint of the LMDz model: map of the partial derivatives, in $\text{ppm}/(\text{kg}/\text{m}^2/\text{h})$, of a weekly mean concentration at site GIF with respect to CO₂ surface fluxes in the previous month during the period 2016-2019. The brown dots denote the location of the surface sites.

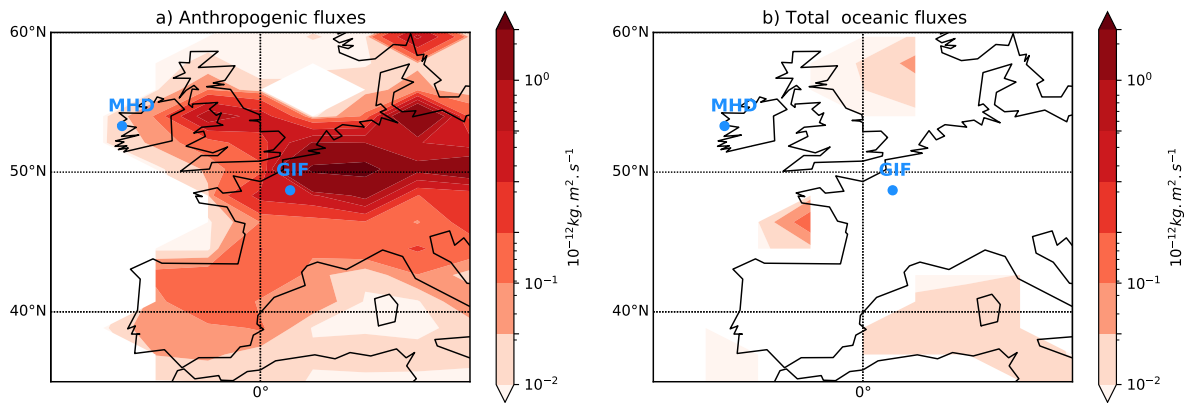


Figure S14. a) Anthropogenic emission map and b) Total oceanic emission map for winter (Dec-Jan-Feb) during the period 2016-2019. The blue dots denote the location of the surface sites. The fluxes have been interpolated on the coarser LMDz grid while ensuring mass conservation. The fluxes are the reference fluxes described in section 2.

References

- Campbell, J. E., Carmichael, G. R., Chai, T., Mena-Carrasco, M., Tang, Y., Blake, D. R., Blake, N. J., Vay, S. A., Collatz, G. J., Baker, I.,
5 Berry, J. A., Montzka, S. A., Sweeney, C., Schnoor, J. L., and Stanier, C. O.: Photosynthetic Control of Atmospheric Carbonyl Sulfide
During the Growing Season, *Science*, 322, 1085–1088, <https://doi.org/10.1126/science.1164015>, <https://science.scienmag.org/content/322/5904/1085>, publisher: American Association for the Advancement of Science Section: Report, 2008.
- Hourdin, F., Talagrand, O., and Idelkadi, A.: Eulerian backtracking of atmospheric tracers. II: Numerical aspects, *Quarterly Journal of the Royal Meteorological Society*, 132, 585–603, <https://doi.org/10.1256/qj.03.198.B>, <https://rmets.onlinelibrary.wiley.com/doi/abs/10.1256/qj.03.198.B>, _eprint: <https://rmets.onlinelibrary.wiley.com/doi/pdf/10.1256/qj.03.198.B>, 2006.
- Ma, J., Kooijmans, L. M. J., Cho, A., Montzka, S. A., Glatthor, N., Worden, J. R., Kuai, L., Atlas, E. L., and Krol, M. C.: Inverse modelling
10 of carbonyl sulfide: implementation, evaluation and implications for the global budget, *Atmospheric Chemistry and Physics Discussions*,
pp. 1–39, <https://doi.org/https://doi.org/10.5194/acp-2020-603>, <https://acp.copernicus.org/preprints/acp-2020-603/>, publisher: Copernicus
GmbH, 2020.
- Montzka, S. A., Calvert, P., Hall, B. D., Elkins, J. W., Conway, T. J., Tans, P. P., and Sweeney, C.: On the global distribution, sea-
sonality, and budget of atmospheric carbonyl sulfide (COS) and some similarities to CO₂, *Journal of Geophysical Research: Atmospheres*,
15 112, <https://doi.org/10.1029/2006JD007665>, <https://agupubs.onlinelibrary.wiley.com/doi/abs/10.1029/2006JD007665>, _eprint:
<https://agupubs.onlinelibrary.wiley.com/doi/pdf/10.1029/2006JD007665>, 2007.
- Van Leer, B.: Towards the ultimate conservative difference scheme. IV. A new approach to numerical convection, *Journal of Computational Physics*, 23, 276–299, [https://doi.org/10.1016/0021-9991\(77\)90095-X](https://doi.org/10.1016/0021-9991(77)90095-X), <http://www.sciencedirect.com/science/article/pii/002199917790095X>, 1977.